Available online at www.sciencedirect.com
ScienceDirect
Journal of Sound and Vibration 301 (2007) 1–17
JOURNAL OF SOUND AND VIBRATION
www.elsevier.com/locate/jsvi

The influence of disk's flexibility on coupling vibration of shaft–disk–blades systems

Chia-Hao Yang[a,b], Shyh-Chin Huang[b,*]

[a]*Instructor of Northern Taiwan Institute of Technology, No. 2, Xueyuan Rd., Peitou, 112 Taipei, Taiwan, ROC*
[b]*Department of Mechanical Engineering, National Taiwan University of Science and Technology, 43, Keelung Road, Sec. 4, Taipei, Taiwan 106, ROC*

Received 1 September 2003; received in revised form 15 September 2004; accepted 27 January 2006
Available online 2 January 2007

Abstract

The coupling vibrations among shaft-torsion, disk-transverse and blade-bending in a shaft–disk–blades unit are investigated. The equations of motion for the shaft–disk–blades unit are first derived from the energy approach in conjunction with the assumed modes method. The effects of disk flexibility, blade's stagger angle and rotational speed upon the natural frequencies and mode shapes are particularly studied. Previous studies have shown that there were four types of coupling modes, the shaft–blade (SB), the shaft–disk–blades (SDBs), the disk–blades (DB) and the blade–blade (BB) in such a unit. The present research focuses on the influence of disk flexibility on the coupling behavior and discovers that disk's flexibility strongly affects the modes bifurcation and the transition of modes. At slightly flexible disk, the BB modes bifurcate into BB and DB modes. As disk goes further flexible, SB modes shift into SDB modes. If it goes furthermore, additional disk-predominating modes are generated and DB modes appear before the SDB mode. Examination of stagger angle β proves that at two extreme cases; at $\beta = 0^\circ$ the shaft and blades coupled but not the disk, and at $\beta = 90^\circ$ the disk and blades coupled but not the shaft. In between, coupling exists among three components. Increasing β may increase or decrease SB modes, depending on which, the disk or shaft's first mode, is more rigid. The natural frequencies of DB modes usually decrease with the increase of β. Rotation effects show that bifurcation, veering and merging phenomena occur due to disk flexibility. Disk flexibility is also observed to induce more critical speeds in the SDBs systems.

1. Introduction

A shaft–disk–blades unit, as shown in Fig. 1, has been widely used in rotating machinery. Applications range from turbine generators, turbine engines, to rotor compressors, etc. Dynamic couplings among shaft, disk and blades could became significant if the disk is flexible and the blade's stagger angle varies. Many researches concerning individual vibrations of shaft, disk and blades have been published worldwide. However, coupling vibrations among shaft torsion, disk transverse and blade bending is rarely addressed. The present research focuses on this issue and explores what extent the coupling relies on disk flexibility and blade's stagger angle.

*Corresponding author. Tel.: +2 27376443; fax: +2 27376460.
E-mail address: schuang@mail.ntust.edu.tw (S.-C. Huang).

0022-460X/$ - see front matter © 2006 Elsevier Ltd. All rights reserved.
doi:10.1016/j.jsv.2006.01.053

Nomenclature

V_{ki}	the ith mode shape of the kth blade
$\hat{v}_{b_k}$	kth blade displacements with respect to the Y_3 axis
v_b, w_b	blade displacements with respect to the Y_2 and Z_2 axes
w_d	disk transverse displacement with respect to the Z_1 axis
β	stagger angle
ϕ	shaft–disk torsional displacement relative to rotation frame
Φ_i, W_i	the ith mode shape of the shaft–disk and disk
$\boldsymbol{q}$, $\boldsymbol{\eta}$, $\boldsymbol{\zeta}$, $\boldsymbol{\xi}$	vectors consisting of generalized coordinates
Ω	rotational speed of shaft speed
Ω^*	dimensionless rotational speed ($\Omega^* = \Omega/\omega_1^b$)
ω_1^b	the first nature frequency of single cantilever blade
ω	natural frequency
ω^*	dimensionless natural frequency ($\omega^* = \omega/\omega_1^b$)

Subscripts

$(\,)_s$	shaft
$(\,)_d$	disk
$(\,)_b$	blade
$(\,)_{ki}$	ith term of the kth blade

Superscripts

$(\,)^n$	n-nodal diameter of disk

Dynamic characteristics of disk flexibility have been studied for years. Lamb and Southwell [1] derived the frequency equations and mode shapes for a circular spinning disk. Southwell [2] extended that investigation to an annular plate clamped inside and free outside in a following paper. Dopkin and Shoup [3] discussed the influence of disks' flexibility on natural frequencies using transfer matrix method. Shen and Ku [4] studied natural frequencies and modes shapes of multiple elastic disks on a rigid shaft through the use of Lagrangian mechanics. The vibration characteristics of the shaft–disk [5–8] and disk–blade [9–12] were studied as well but not the coupling effects among components were discussed. Chivens and Nelson [13] investigated the influence of disk flexibility on bending natural frequencies and critical speeds of a flexible shaft–disk system using the Laplace transform method. They concluded that critical speeds were insignificant to disk flexibility, but natural frequencies did. Shahab and Thomas [14] discussed the coupling effects of shaft and disk flexibility on a shaft-multiple disks system using the finite element method. Their investigation revealed that disk rigidity imposed less effect than shaft on system modes. Shen [15] used the assumed modes method to study the natural frequencies and mode shapes of a shaft-multiple disks system on forced vibration. Wu and Flowers [16] investigated the coupling effects of shaft and disk using the transfer matrix method. Jia et al. [17] used the assumed mode method to investigate the longitudinal coupled vibration of a flexible shaft with multiple flexible disks. Lee and Chun [18] investigated the effects of multiple flexible disks on the vibration modes of a flexible shaft–disk system via using assumed modes method. The frequency bifurcations of shaft and disk coupling modes occurred due to disk flexibility. Omprakash and Ramamurti [19] analyzed the natural frequencies of rotating disk–blade system by a combined cycle symmetry and Rayleigh–Ritz method. Omprakash and Ramamurti [20] discussed the influence of stagger and pretwist angle on the coupling vibration characteristics of disk–blade system by the finite element method. They investigated the influence of disk flexibility and found that disk–blades coupling frequencies approached the blade's frequencies as the number of disk's nodal diameters increased. When the stagger angle was zero, the disk and blades were completely uncoupled. As to the dynamic characteristics of a shaft–disk–blades unit, there were limited investigations in the existing literature. Khader and Loewy [21] discussed the forced response of a rotating shaft–disk–blades system by modal analysis method and focused on the influence of Coriolis force. Sakata et al. [22] investigated the influence of gyroscopic moment of the shaft–disk–blades system by the finite element method. Chun and Lee [23] used the assumed mode method to investigate the influence of the forces and torques, resulted from changes of blade's stagger and pretwist angles, on the dynamic coupling of a flexible shaft–disk–blades unit. This investigation had arrived at some conclusions: the pretwist angle had far less influence on the system dynamics than the stagger angle, and the torque and coupling effect on the shaft

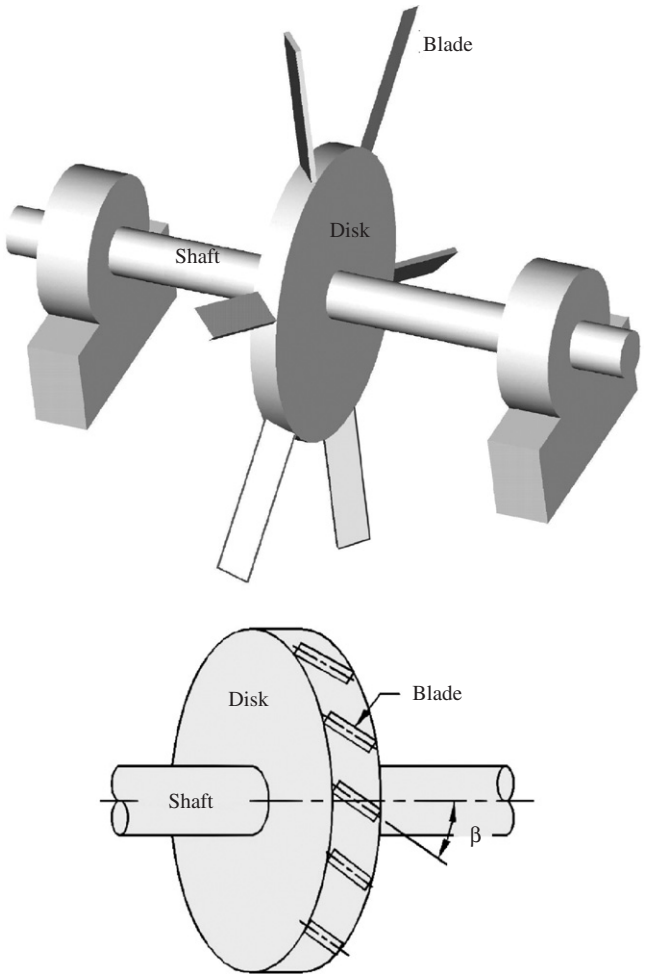

Fig. 1. A typical shaft–disk–blades system.

became the larger with the decrease of stagger angle but was in an opposite way onto the disk. All the above researches addressed on the bending and longitudinal vibration of shaft, not the torsion. Huang and Ho [24] pioneered the investigation of coupling modes between shaft torsion and blade bending in a shaft–disk–blades unit via the receptance method. But the disk was reasonably assumed rigid due to zero stagger angle. Recently, the authors [25] extended Huang and Ho's work to include disk flexibility at nonzero stagger angle. They discovered that there existed four types of coupling modes, said shaft–blade (SB), blades–blades (BBs), disk–blades (DBs) and shaft–disk–blades (SDBs) modes. The present research looks more into the influence of disk flexibility and blade's stagger angle on the coupling behavior.

The SDB system considered herein has N_b-flexible blades clamped into a flexible disk with a stagger angle (β) and the shaft undergoes torsion vibration around a constant rotating axis. In this paper, the authors employed the energy approach and the assumed modes method for analytical studies. The case of five blades is illustrated as examples. Frequency diagrams and mode shapes are given to help realizing and interpreting the coupling phenomena.

2. Theoretical analysis

Fig. 1 shows a typical SDB system to be discussed. Due to blade flexibility, the blade vibration will transmit to the disk and subsequently induces the disk's transverse vibration (if $\beta \neq 0$). The disk's in-plane motion will

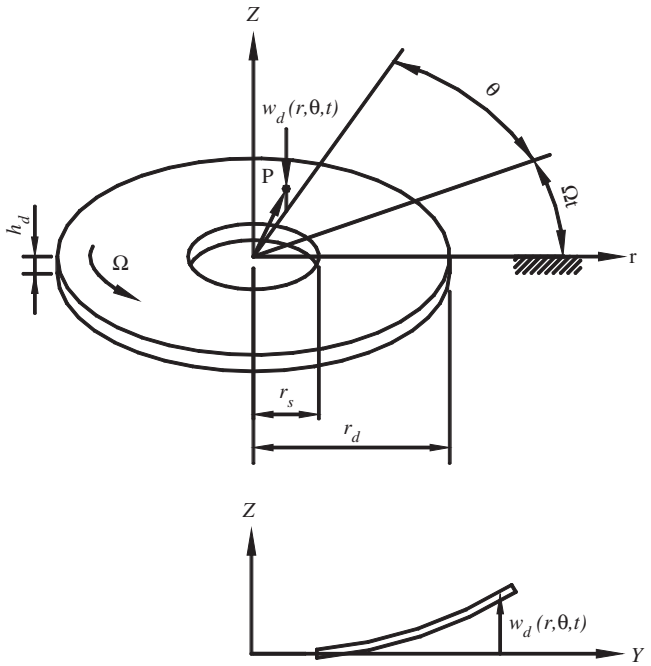

Fig. 2. The geometry and coordinate systems of the rotating disk.

also cause the shaft's torsional vibration. In a reverse way, the shaft's torsional vibration will drive the vibrations of disk and blades as well. All these subsequences complicate the vibration behavior among all components. In the following theoretical analysis, the authors intend to look more into the coupling vibrations, particularly due to disk flexibility. Two assumptions are made prior to the analysis. First, the disk is in-plane rigid as compared to its transverse vibration and shaft's torsion. Second, the initial stresses in the disk and blades due to rotation are accounted only to the constant spin speed Ω, since the torsional vibration $\dot{\phi}$ is much smaller than Ω and can be reasonably neglected. The analyses begin with the energy derivations for all subsystems. Then, the assumed-modes method follows to discretize equations.

2.1. Energy functions

The total energy of the SDB system is decomposed into the energy of shaft–disk and that of blades. The energy associated with shaft–disk consists of the shaft–disk's torsional and the disk's transverse vibration. The torsional displacement with respect to the constantly rotating frame is denoted $\phi(Z,t)$. Fig. 2 illustrates a rotating disk with clamped inside and free outside. r_s, r_d and h_d denote the disk's inner, outer radius and thickness, respectively. w_d denotes the disk's transverse displacement.

The kinetic and strain energies associated with shaft–disk are

$$T_s = \frac{1}{2}\int_0^{L_s} I_s\left(\dot{\phi}+\Omega\right)^2 \mathrm{d}Z + \frac{I_d}{2}\left(\dot{\phi}+\Omega\right)^2\Big|_{Z=Z_d}, \tag{1}$$

$$T_d = \frac{\rho_d h_d}{2}\int_{r_s}^{r_d}\int_0^{2\pi}\left(\dot{w}_d + \Omega\frac{\partial w_d}{\partial\theta}\right)^2 r\,\mathrm{d}\theta\,\mathrm{d}r, \tag{2}$$

$$U_s = \frac{1}{2}\int_0^{L_s} G_s J_s\left(\frac{\partial\phi}{\partial Z}\right)^2 \mathrm{d}Z, \tag{3}$$

$$U_d = \frac{D}{2}\int_{r_s}^{r_d}\int_0^{2\pi}\left\{\left(\nabla^2 w_d\right)^2 - 2(1-\nu)\frac{\partial^2 w_d}{\partial r^2}\left[\left(\frac{1}{r}\frac{\partial w_d}{\partial r}+\frac{1}{r^2}\frac{\partial^2 w_d}{\partial \theta^2}\right)\right.\right.$$
$$\left.\left.-\left(\frac{1}{r}\frac{\partial^2 w_d}{\partial r\partial\theta}-\frac{1}{r^2}\frac{\partial w_d}{\partial\theta}\right)^2\right]\right\} r\,\mathrm{d}r\,\mathrm{d}\theta$$
$$+\frac{h_d}{2}\int_{r_s}^{r_d}\int_0^{2\pi}\left[\sigma_r\left(\frac{\partial w_d}{\partial r}\right)^2+\sigma_\theta\left(\frac{1}{r}\frac{\partial w_d}{\partial\theta}\right)^2\right] r\,\mathrm{d}r\,\mathrm{d}\theta, \tag{4}$$

where L_s, I_s, and G_sJ_s denote the shaft's length, polar rotatary inertia, and torsional rigidity, respectively. I_d is the disk's polar rotatary inertia. The upper *dot* denotes time derivatives and subscripts s and d designate shaft and disk, respectively. ∇^2 is the Laplacian. D is the bending rigidity. σ_r and σ_θ are the initial stresses due to rotation in radial and circumferential directions. Detail expressions are given in Appendix A.

Fig. 3 shows a typical rotating blade cantilevered into a flexible disk with a stagger angle β. The (X, Y, Z) coordinate system is the inertia frame; the (x_1, y_1, z_1) frame rotates at a constant speed Ω. The (x_2, y_2, z_2) frame orients an angle β relative to the (x_1, y_1, z_1) frame, and the (x_3, y_3, z_3) frame is fixed to the blade's root. The v_b and w_b are the transverse displacements of the blade in y_2 and z_2 directions, respectively.

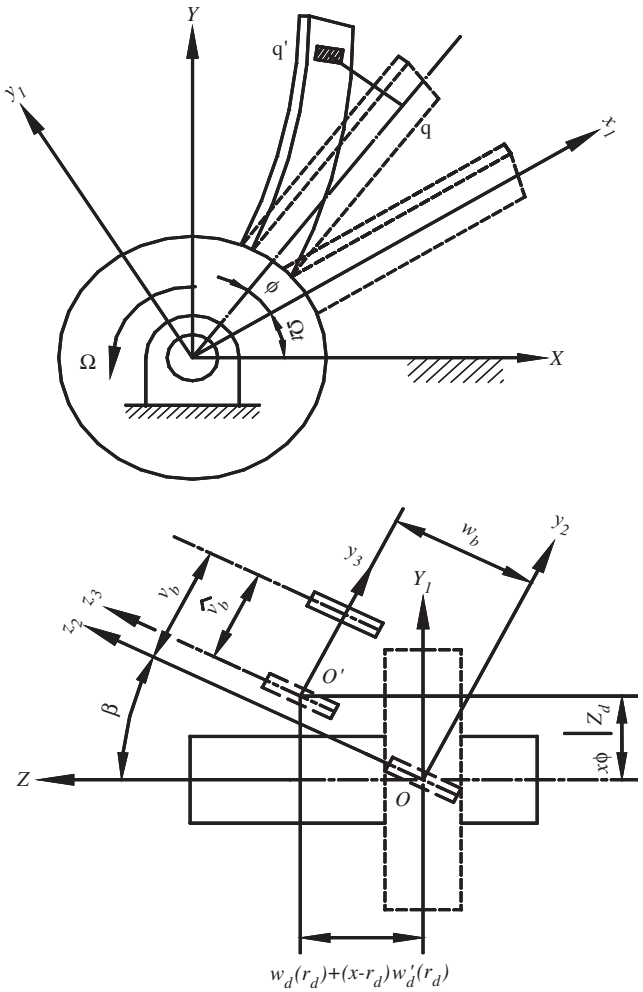

Fig. 3. Blade's coordinate systems and deformation.

The kinetic and strain energies associated with a blade are

$$T_b = \frac{1}{2}\int_{r_d}^{r_b} \rho_b A_b \{\dot{v}_b^2 + \dot{w}_b^2 + (v_b \cos\beta + w_b \sin\beta)^2\Omega^2 + x^2\Omega^2 + 2x(\dot{v}_b \cos\beta + \dot{w}_b \sin\beta)\Omega\}\,\mathrm{d}x + \frac{1}{2}\int_{r_d}^{r_b} I_b\left(\Omega\cos\beta + \frac{\partial \dot{v}_b}{\partial x}\right)^2 \mathrm{d}x, \tag{5}$$

$$U_b = \int_{r_d}^{r_b} \frac{E_b I_A}{2}\left(\frac{\partial^2 v_b}{\partial x^2}\right)^2 \mathrm{d}x + \int_{r_d}^{r_b} \frac{\Omega^2 \rho_b A_b}{4}(r_b^2 - x^2)\left[\left(\frac{\partial v_b}{\partial x}\right)^2 + \left(\frac{\partial w_b}{\partial x}\right)^2\right]\mathrm{d}x. \tag{6}$$

where I_A is the area moment of inertia about z_3 axis, and I_b is polar moment of inertia.

The total displacements of a blade, $v_b(x,t)$ and $w_b(x,t)$ consist of the shaft's torsional displacement $\phi(Z_d,t)$, the disk's transverse displacement w_d, and the blade's bending displacement $\hat{v}_b(x,t)$. The kinematic relations between these displacements are

$$v_{b_k}(x_k,t) = \hat{v}_{b_k} + x_k\phi\big|_{Z_d}\cos\beta - \left(w_d|_{r_d} + x_k w_d'\big|_{r_d}\right)\sin\beta, \tag{7}$$

$$w_{b_k}(x_k,t) = x_k\phi\big|_{Z_d}\sin\beta + \left(w_d|_{r_d} + x_k w_d'\big|_{r_d}\right)\cos\beta, \tag{8}$$

where the subscript k denotes the kth blade.

2.2. Equations of motion

Hamilton's principle may be applied to yield the equations of motion in a continuous fashion from the above energies. However, direct solutions to the continuous equations are impractical and inefficient, if not impossible. A discretization process via assumed-modes method is hence employed. The mode shapes of the corresponding nonrotating components are adopted as the trial functions, i.e.,

$$\phi(Z,t) = \sum_{i=1}^{n_s} \Phi_i(Z)\eta_i(t) = \mathbf{\Phi}(Z)\boldsymbol{\eta}(t), \tag{9}$$

$$w_d(r,\theta,t) = \sum_{i=1}^{n_d} W_i(r,\theta)\zeta_i(t) = \mathbf{W}(r,\theta)\boldsymbol{\zeta}(t), \tag{10}$$

$$\hat{v}_{b_k}(x_k,t) = \sum_{i=1}^{n_b} V_{ki}(x_k)\xi_{ki}(t) = \mathbf{V}_k(x_k)\boldsymbol{\xi}_k(t), \tag{11}$$

where Φ_i, W_i and V_{ki} are the mode shapes of a shaft, a disk and a blade, respectively. η_i, ζ_i and ξ_{ki} are the corresponding participation factors. n's with the subscripts for the corresponding subsystems, are the numbers of modes deemed necessary for required accuracy.

Substitution of the above equations into the energy expressions and employing the Lagrange equations yields the following discretizated equations of motion in matrix notation as

$$\mathbf{M}\ddot{\mathbf{q}} - \Omega\mathbf{P}\dot{\mathbf{q}} + (\mathbf{K}^e + \mathbf{K}^i - \Omega^2\mathbf{K}^\Omega)\mathbf{q} = 0, \tag{12}$$

where the above matrices $\mathbf{M}$, $\mathbf{P}$, $\mathbf{K}^e$, $\mathbf{K}^i$, and $\mathbf{K}^\Omega$ are listed in Appendix A. $-\Omega\mathbf{P}$, generated from the Coriolis effect, because of flexible disk, induces the bifurcation phenomenon of natural frequencies [26]. $\mathbf{K}^e$, arising from the elastic deflection, dominates at low rotational speed. $\mathbf{K}^i$ comes from the initial stress. The term $-\Omega^2\mathbf{K}^\Omega$ comes from rotation and softens the rotor at high speed. $\mathbf{q}$ is the generalized vector, i.e.,

$$\mathbf{q} = \{\boldsymbol{\eta}\backslash\boldsymbol{\zeta}\backslash\boldsymbol{\xi}\}^{\mathrm{T}}. \tag{13}$$

The natural frequencies and mode shapes can now be solved for and the corresponding coupled behavior can be studied.

3. Numerical results

The system's mode shapes at which the blade's first mode predominates are illustrated in the following examples. To help discussing the influence of disk flexibility upon the coupling vibrations, the authors define a coupling factor $R_c = (E_b I_A)/[D(r_b - r_d)]$. R_c denotes a rigidity ratio of blade to disk. As R_c approaches zero, it implies the disk is much more rigid than the blade, and for such a case the blades and disk can be treated as fully uncoupled as usual. At the threshold the disk flexibility induces coupling phenomenon the corresponding coupling factor is here called the critical coupling factor, denoted R_c^c. Notably, R_c^c varies with stagger angle β as Fig. 4 shows. From Fig. 4, it is seen that larger β brings larger coupling between blade and disk (smaller R_c^c). Table 1 lists the geometric and material properties of the illustrated examples. Note that, the sizes of disk and blades are exaggerated in these cases to magnify the coupling effects. To avoid dimensional dependence, the shown results are normalized with respect to the cantilevered blade's first natural frequency ($\omega_1^b = 81.538$ Hz), i.e., $\omega^* = \omega/\omega_1^b$ and $\Omega^* = \Omega/\omega_1^b$. Similarly, a dimensionless coupling factor is defined as the ratio of coupling factor to its corresponding critical coupling factor, i.e., $R^* = R_c/R_c^c$. The threshold of disk coupling for all β cases occurs at $R^* = 1$. In order to identify the influence of disk flexibility on the coupling vibration, the

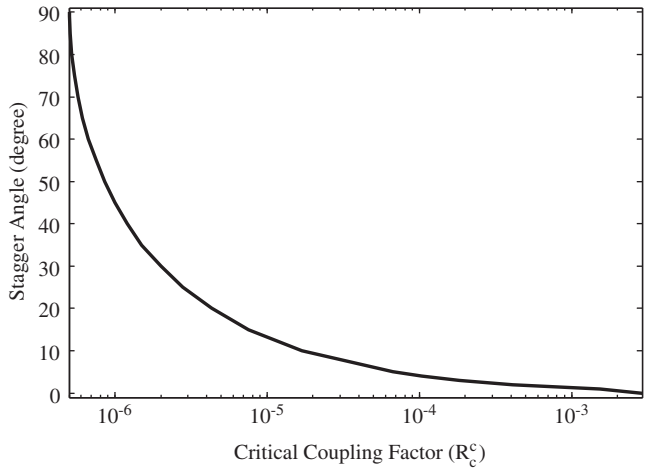

Fig. 4. Variations of R_c^c to stagger angle β.

Table 1
Geometric and material properties of the illustrated examples

Shaft	Density: ρ_s	7850 kg/m^3
	Shear modulus: G_s	75 GPa
	Shaft length: L_s	0.6 m
	Radius: r_s	0.04 m
Disk	Location: z_d	0.3 m
	Radius: r_d	0.2 m
	Poisson's ratio: v	0.3
	Mass of disk: M_d	28.41 kg
Blade	Density: ρ_b	7850 kg/m^3
	Young's modulus: E_b	200 GPa
	Blade outer end: r_b	0.4 m
	Cross-section: A_b	1.2×10^{-4} m^2
	area moment of inertia: I_A	1.92×10^{-9} m^4
	mass moment of inertia: I_b	1.51×10^{-5} m^4
Dimensionless rotational speed: Ω^*		0–12

natural frequencies of disk with various disk flexibility (represented by R^*) are first calculated and illustrated in Fig. 5. In the following, the cases of five blades are demonstrated as numerical examples. Huang and Ho [24] once investigated the coupling modes of SDB unit with a rigid disk and $\beta = 0$, and discovered that the coupling modes could be grouped into two categories, the SBs coupling and the BBs coupling.

Figs. 6–8 illustrate the first three mode shapes of a five-blade system with stagger angle $\beta = 30^\circ$. The first x–y plot denotes the torsional displacement of the shaft. The following plots show the deformation of disk and blades. Fig. 6 shows the mode shapes at the threshold case of $R^* = 1$. In this case, the disk's participation is negligible (no deformation), there exist therefore only SB and BB modes. At the mode #1 the blade's first bending mode predominates, and at mode #3 the shaft's first torsional mode predominates. Mode #2 is a BB mode (no shaft torsion) and it occurs always at repeated frequencies [24]. Fig. 7 shows the mode shapes of $R^* = 2.8$. Two extra modes, denoted #2a and #2b, are bifurcated from the original BB mode (#2). These two modes are associated with disk's 1- and 0-nodal diameter modes but there is no shaft torsion, hence classified as DB modes. The first phenomenon arising from disk flexibility is here observed to be the bifurcation from the original BB mode (#2) into BB (#2) and DB (#2a, #2b) modes. When R^* continues increasing, as Fig. 8

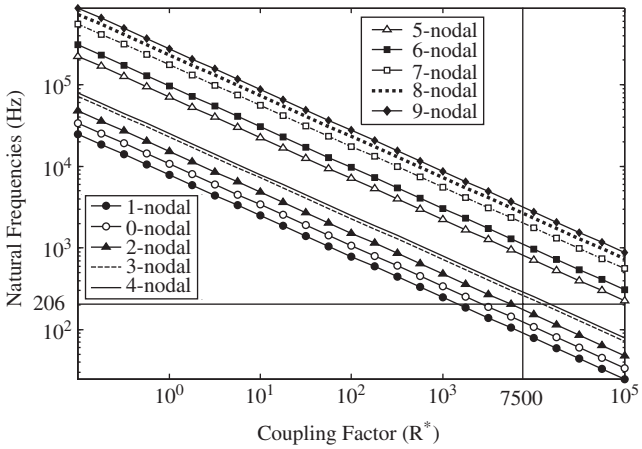

Fig. 5. Variations of disk's frequencies to various disk flexibility.

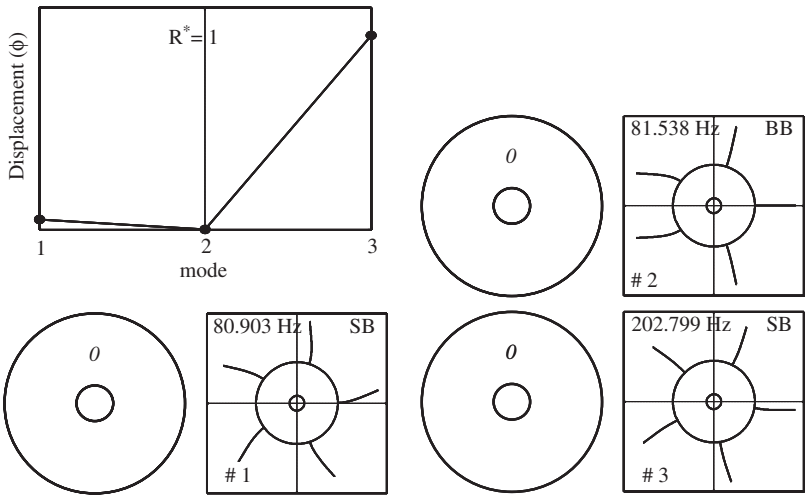

Fig. 6. The mode shapes of the blade's first mode predominate for $\beta = 30^\circ$ and $R^* = 1$.

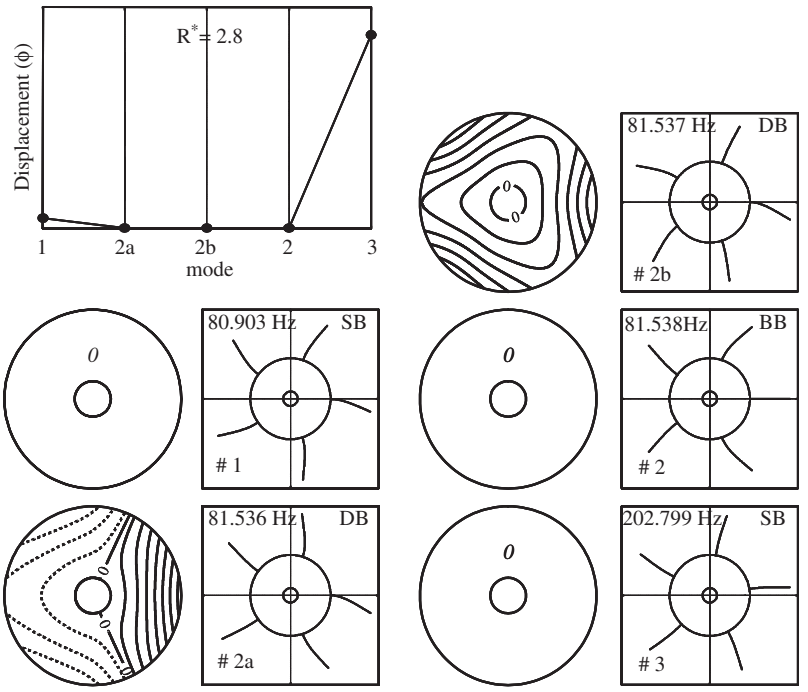

Fig. 7. The mode shapes of the blade's first mode predominate for $\beta = 30^\circ$ and $R^* = 2.8$.

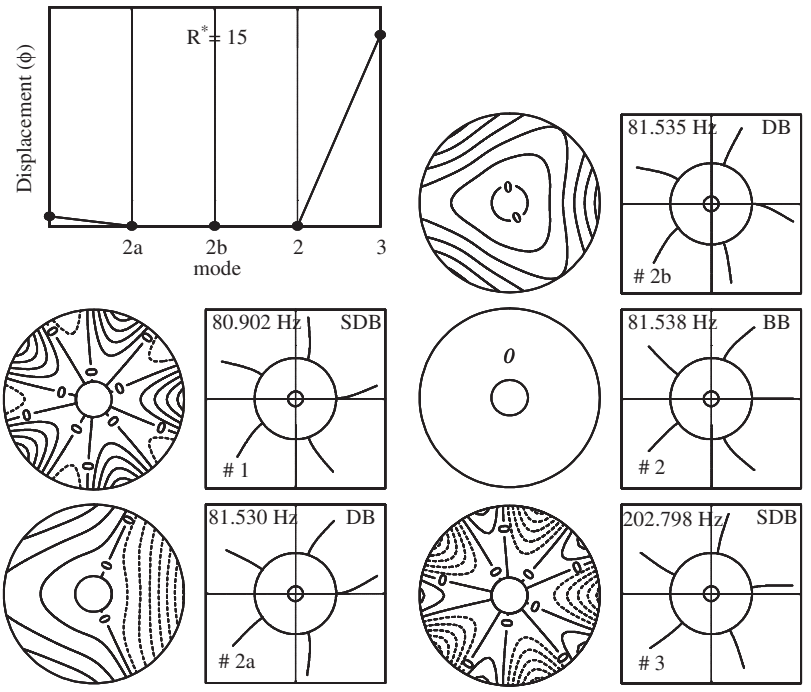

Fig. 8. The mode shapes of the blade's first mode predominate for $\beta = 30^\circ$ and $R^* = 15$.

shows for $R^* = 15$, the second phenomenon happens, i.e., SB modes (#1, #3) transfer into SDB modes. In this example, modes#1, #2a, #2b and #2 are very similar to those of Fig. 7 except for slightly lower natural frequencies at DB modes due to more flexibile disk. Note that, modes #2a, #2b, and #2 in Figs. 7 and 8 are

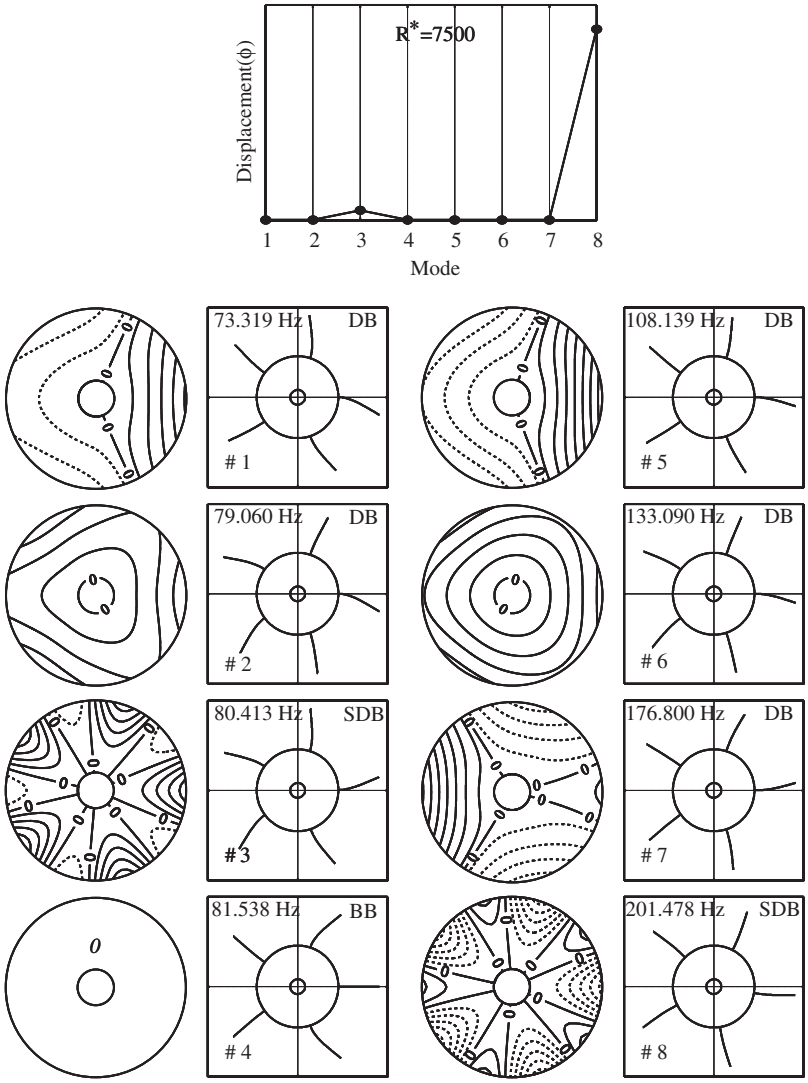

Fig. 9. The mode shapes of the blade's first mode predominate for $\beta = 30^\circ$ and $R^* = 7500$.

very close in both deformation and frequency. It is because that the three modes are rooted from the original BB mode with repeated frequencies in which the blades' first bending mode dominates in a rigid disk case. The entering of disk flexibility reduces the BB mode's multiplicity and induces two more modes #2a and #2b.

With R^* increasing further, e.g., $R^* = 7500$, as Fig. 9 shows, the disk's lowest three natural frequencies fall below the shaft's first torsional frequency, said 206 Hz in the example. The disk's rather than the blade's or the shaft's predominant modes appear. Modes #1 and #2 are those of the DB modes evolved from the original repeated BB mode. Modes #3 and #8 are similar to modes #1 and #3 of Fig. 8 except with lower natural frequencies. The modes #1 (73.319 Hz) and #5 (108.319 Hz) shown in Fig. 9 are very similar, but the mode #1 is predominated by blade's first mode, and mode #5 is by the disk's mode. Similarity appears at modes #2 and #6. Their differences may be told by contrasting the disk's deformation contours. Modes #5 and #6 apparently exist larger disk deformation than modes #1 and #2. In this figure, two phenomena are observed. First, there are three extra modes (#5, #6 and #7) generated from original disk's modes. Second, the DB modes fall below the SDB mode and become the lowest modes. The second phenomenon is physically realized to be attributed

to the disk's more flexibility than the shaft. To explain these three modes one may address back to Fig. 5 and notice that at $R^* = 7500$, three disk modes, corresponding to $n = 1$, 0 and 2, fall below 206 Hz, the first torsional mode. They are exactly, in sequence, the bifurcated modes #5, #6 and #7 of Fig. 9.

The above examples reveal a fact that disk's flexibility not only decreases the system's natural frequencies but also alters the number of modes. In order to realize how the modes bifurcated with R^*, the loci of modes for four β values are shown in Fig. 10. In this figure, the solid symbols represent the modes predominated by blade, and hollow symbols represent the modes predominated by shaft or by disk. The superscript "n" in disk coupling modes represented the associated disk's n-nodal diameter mode. Fig. 10(a) shows the case of $\beta = 0^\circ$. At R^* less than 1, there exist SB and BB modes and it is consistent with Huang and Ho's [24] via receptance approach. With the increase of R^* the frequencies loci of BB and SB branches do not bifurcate neither veer. It is because at this stagger angle, the disk's transverse is completely uncoupled with the blades and the shaft.

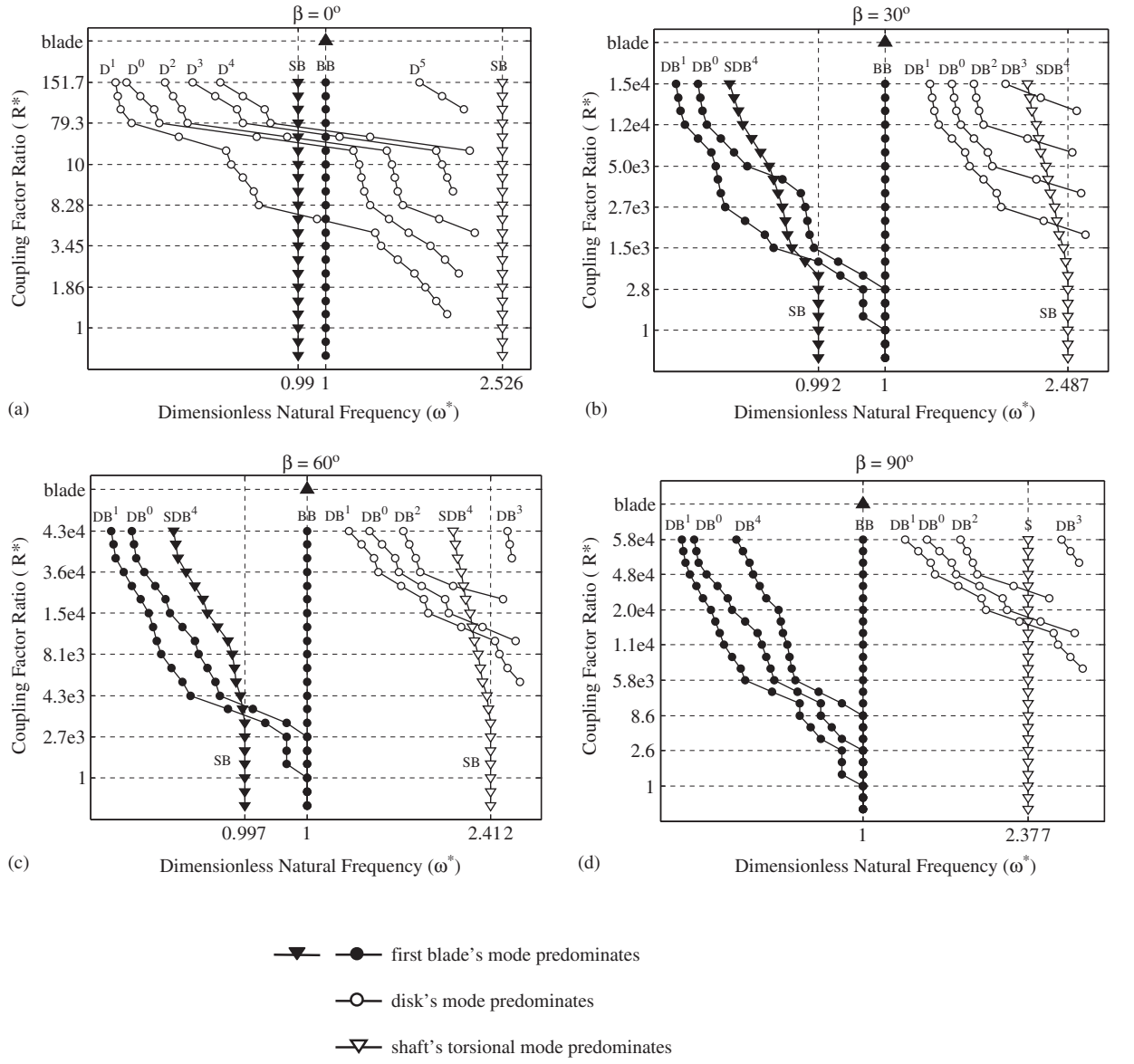

Fig. 10. Variations of the combined system's frequencies on the R^*: (a) for $\beta = 0^\circ$; (b) for $\beta = 30^\circ$; (c) for $\beta = 60^\circ$; and (d) for $\beta = 90^\circ$.

The disk's frequency loci, marked with symbol D, exist independently, and bend to the left (less) with increasing R^*. When $0<\beta<90^\circ$, the force acting on disk's transverse direction is no longer zero. The disk is hence coupled with the blades and the shaft. Figs. 10(b) and 10(c) show the cases of $\beta = 30^\circ$ and 60°. As R^* exceeds 1 the BB locus, represented by solid dots, not only retains its original BB branch but also bifurcates into DB^1 and DB^0 branches. The SB locus, represented by triangle symbols, bends to the left and eventually become SDB modes as R^* increases. The disk-predominating DB modes, circle symbols, appear as R^* reaches certain values, e.g., $R^*>1500$ for $\beta = 30^\circ$. Fig. 10(d) shows an extreme case of $\beta = 90^\circ$, in which blades and disk are fully coupled but completely uncoupled to the shaft because no net torques onto shaft's torsional direction. The shaft's torsional frequency loci, marked with "S", do not vary with R^*. The bifurcation phenomena of BB modes are similar to the previous cases.

The effects of stagger angle β on the coupling frequencies are next to be examined. In order to realize disk's effect, the authors choose two values for R_c, one is the disk being more rigid than shaft's first torsional frequency and the other is the opposite. Fig. 11(a) represents an example of rigid disk ($R_c = 9\times10^{-6}$). $R_c = 9\times10^{-6}$ is the critical coupling factor for $\beta = 13^\circ$. Therefore, as β is less than 13°, there is no bifurcation in BB locus. As to the first SB mode locus, it is seen that with the increase of β the frequency locus bends to the right (larger). It is due to the disk is more rigid than the shaft's first torsional mode and larger β means more participation of disk than the shaft. To the opposite case, Fig. 11(b) shows that the first SB branch bends to the left as expected. As to the second branch of SB mode both loci bend to the left (smaller) as β increases. As to the bifurcated DB loci, it is seen that the increase of β implies more disk participation and less shaft and blades, so DB frequencies decrease. The D modes loci in Fig. 11(b), however, increase with β and eventually transfer into DB modes. Fig. 11 also shows how the coupling modes transit with the stagger angle.

At last, the authors examine the effect of shaft rotational speed on system's natural frequencies. Figs. 12(a)–(d) show the effect of rotational speed on natural frequencies for different β values with a relatively rigid disk. In this case, the frequency bifurcation due to rotation is not clear and only the positive natural frequencies are shown in figures. The BB frequencies increase with rotation due to centrifugal forces. At $\Omega^* = 8.5$, the loci of shaft related modes intersects the abscissa ($\omega = 0$), these intersections are customarily

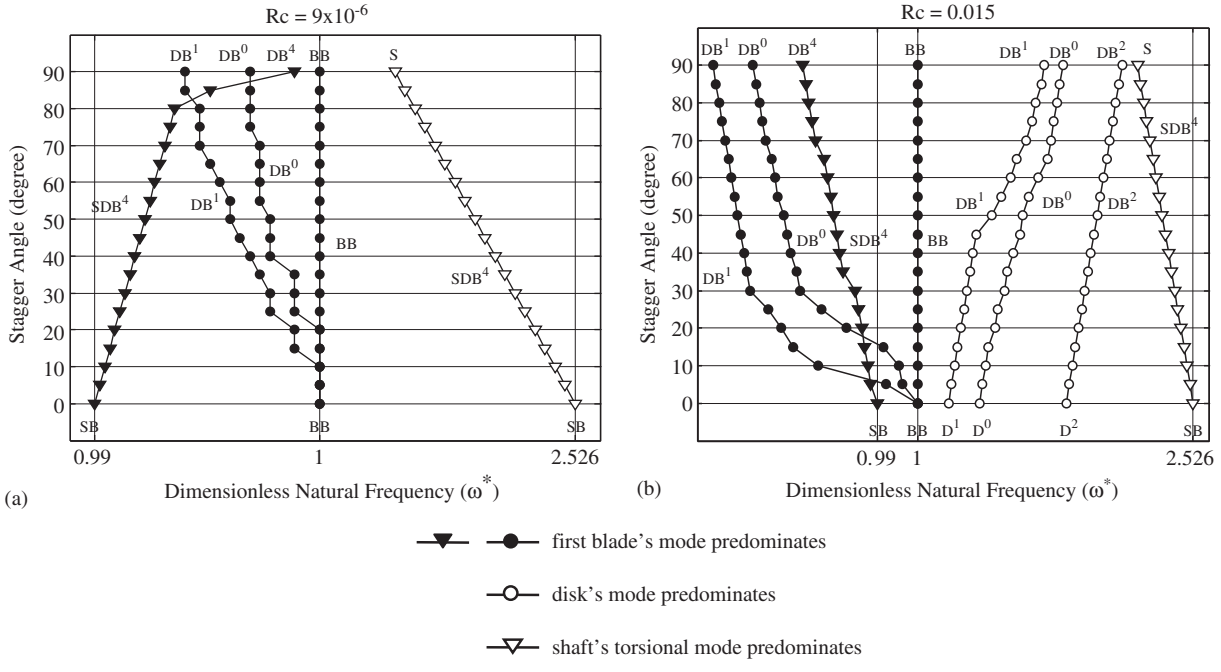

Fig. 11. Variations of the combined system's frequencies on the β: (a) for $R_c = 9\times10^{-6}$; and (b) for $R_c = 0.015$.

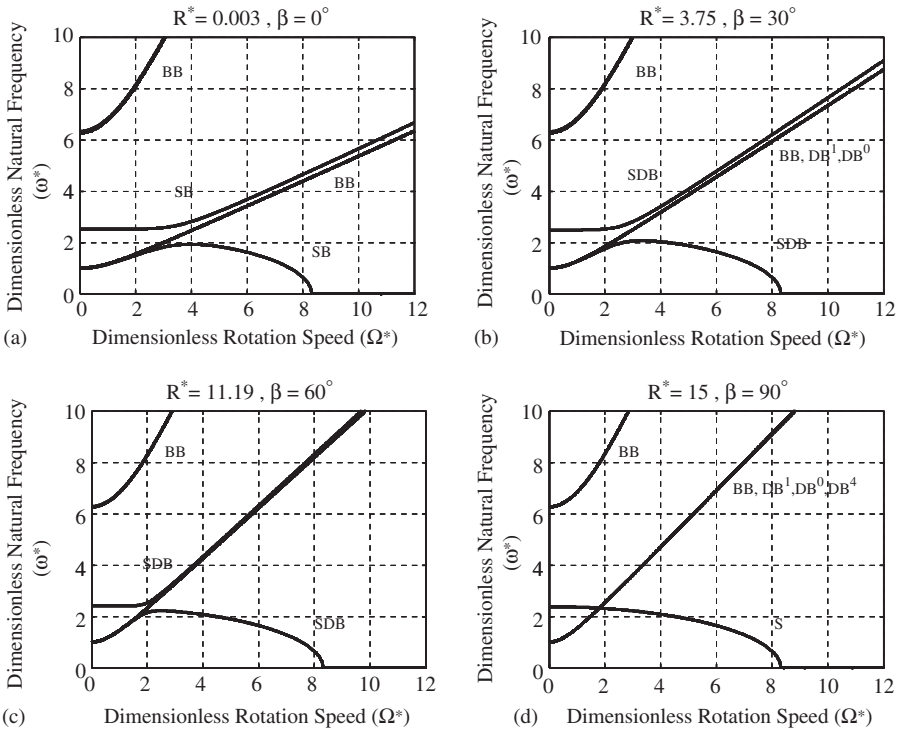

Fig. 12. Variation of natural frequencies with rotation speed of $R_c = 9 \times 10^{-6}$: (a) for $\beta = 0°$; (b) for $\beta = 30°$; (c) for $\beta = 60°$; and (d) for $\beta = 90°$.

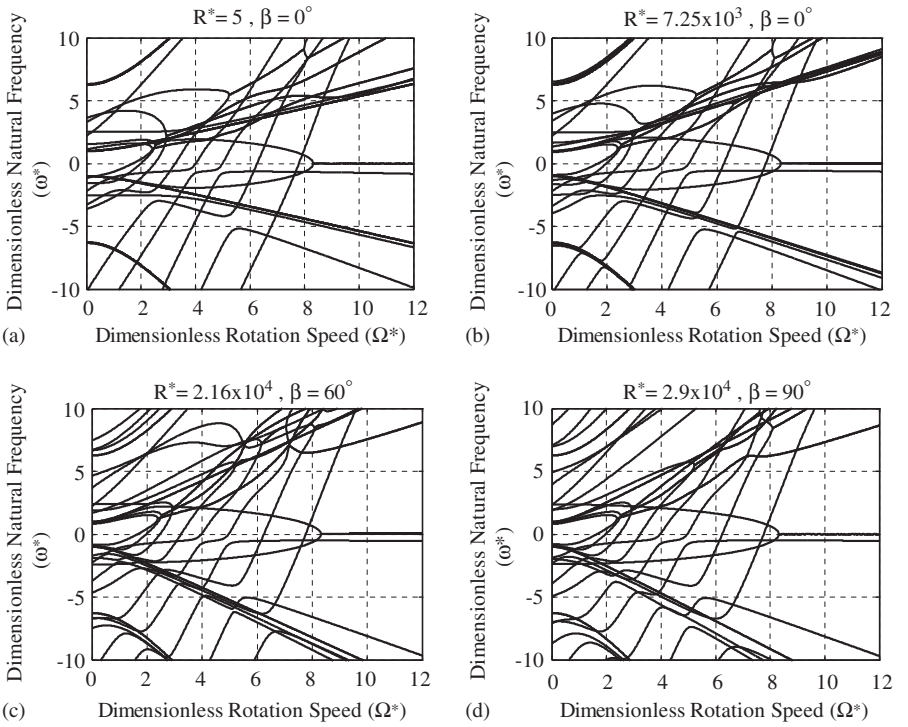

Fig. 13. Variation of natural frequencies with rotation speed of $R_c = 0.015$: (a) for $\beta = 0°$; (b) for $\beta = 30°$; (c) for $\beta = 60°$; and (d) for $\beta = 90°$.

referred as system's critical rotational speeds, which belong to the divergent type of instability. Eq. (12) showed that it could happen as $-\Omega^2\mathbf{K}^{\Omega}$ was large enough. Further examination of the condition, it is found that those critical speeds are attributed to Eq. (A.20), that is irrelevant to β and disk. Figs. 13(a)–(d) are intended to show the bifurcation of modes due to flexible disk and rotation. The flexible rotor system frequently exist loci bifurcation, veering and merging phenomena. It is also noted that there are more critical speeds than previous case, one is the shaft-related and the others are disk-related. In these figures, there exist mode exchange (loci crossings) and instability problems (intersections with abscissa), and are very complicated phenomena. The figure is just showing the mutual effects of disk flexibility and rotation as compared to Fig. 12. No intension is made in this research to look into those phenomena.

4. Conclusions

The equations of the SDB unit are derived from the energy approach in conjunction with the assumed modes method. Numerical results with the emphases on disk flexibility, stagger angle and rotational speed are illustrated. The authors have arrived at the following conclusions from the studies.

At R^* less than 1, the disk's participation is negligible, there exist only SB and BB modes. As R^* keeps increasing, the phenomena occur in the following sequence: (1) The BB modes bifurcate into DB and BB modes. (2) The SB modes shift into SDB modes. (3) As disk's flexibility falls below the shaft's first mode, disk-predominating modes are generated and the DB mode replacing SDB mode becomes the lowest mode.

The blade's stagger angle β has shown the following effects on system's mode shapes and natural frequencies. When $\beta = 0$, disk's transverse flexibility imposes no effect on system's dynamic characteristic. It hence can be assumed a rigid disk as Huang and Ho's [24]. At $\beta = 90^\circ$, shaft's torsion does not participate in coupling modes. As β ranges from 0° to 90°, the authors have arrived at the following from frequency loci: (1) As the disk is more rigid than the shaft's first torsional frequency, the first SB mode locus bends to the right (larger) with increasing β. To the opposite case, the first SB mode locus bends to the left (smaller). (2) The DB modes frequency loci decrease with β. (3) The D modes loci increase with β and eventually transfer into DB modes.

As Ω^* keeps increasing, the phenomena of bifurcating and merging of frequency loci occur. From the illustrated examples, some conclusions can be drawn: (1) The frequency bifurcations due to rotation occur as the disk is relatively flexible. (2) Most of the critical rotational speeds result from disk's flexibility. (3) There exist modes exchange, loci veering and even stability consideration and these would be worth investigation in the future.

Appendix A

The Laplacian and bending rigidity are defined as

$$\nabla^2 = \frac{\partial^2}{\partial r^2} + \frac{\partial}{r\partial r} + \frac{\partial^2}{r^2\partial\theta^2}, \tag{A.1}$$

$$D = \frac{E_d h_d^3}{12(1-\nu^2)}. \tag{A.2}$$

The initial stress are defined as

$$\sigma_r = \frac{3+\nu}{8}\rho_d\Omega^2(r_d^2 - r^2) + \frac{(1-\nu)\rho_d\Omega^2 r_s^2\left[(3+\nu)r_d^2 - (1+\nu)r_s^2\right]}{8\left[(1+\nu)r_d^2 + (1-\nu)r_s^2\right]}\left(\frac{r_d^2}{r^2} - 1\right), \tag{A.3}$$

$$\sigma_\theta = \frac{\Omega^2}{8}\left[(3+\nu)r_d^2 - (1+3\nu)r^2\right] - \frac{(1-\nu)\rho_d\Omega^2 r_s^2\left[(3+\nu)r_d^2 - (1+\nu)r_s^2\right]}{8\left[(1+\nu)r_d^2 + (1-\nu)r_s^2\right]}\left(\frac{r_d^2}{r^2} + 1\right). \tag{A.4}$$

The matrices are expressed as

$$\mathbf{M}=\begin{bmatrix} \mathbf{M}_{ss} & 0 & \mathbf{M}_{sb_1} & \cdots & \mathbf{M}_{sb_{Nb}} \\ 0 & \mathbf{M}_{dd} & \mathbf{M}_{db_1} & \cdots & \mathbf{M}_{sb_{Nb}} \\ \mathbf{M}_{sb_1}^{\mathrm{T}} & \mathbf{M}_{db_1}^{\mathrm{T}} & \mathbf{M}_{b_1b_1} & 0 & 0 \\ \vdots & \vdots & 0 & \ddots & 0 \\ \mathbf{M}_{sb_{Nb}}^{\mathrm{T}} & \mathbf{M}_{db_{Nb}}^{\mathrm{T}} & 0 & 0 & \mathbf{M}_{b_{Nb}b_{Nb}} \end{bmatrix}, \tag{A.5}$$

$$\mathbf{P}=\begin{bmatrix} 0 & 0 & 0 & \cdots & 0 \\ 0 & \mathbf{P}_{dd} & 0 & \cdots & 0 \\ 0 & 0 & 0 & \ddots & \vdots \\ \vdots & \vdots & \ddots & \ddots & 0 \\ 0 & 0 & \cdots & 0 & 0 \end{bmatrix}, \tag{A.6}$$

$$\mathbf{K}^{e}=\begin{bmatrix} \mathbf{K}_{ss}^{e} & 0 & \cdots & \cdots & 0 \\ 0 & \mathbf{K}_{dd}^{e} & 0 & \cdots & \vdots \\ \vdots & 0 & \mathbf{K}_{b_1b_1}^{e} & 0 & \vdots \\ \vdots & \vdots & 0 & \ddots & 0 \\ 0 & \cdots & \cdots & 0 & \mathbf{K}_{b_{Nb}b_{Nb}}^{e} \end{bmatrix}, \tag{A.7}$$

$$\mathbf{K}^{i}=\begin{bmatrix} 0 & 0 & \cdots & \cdots & 0 \\ 0 & \mathbf{K}_{dd}^{i} & 0 & \cdots & \vdots \\ \vdots & 0 & 0 & \cdots & \vdots \\ \vdots & \vdots & \vdots & \ddots & \vdots \\ 0 & \cdots & \cdots & \cdots & 0 \end{bmatrix}, \tag{A.8}$$

$$\mathbf{K}^{\Omega}=\begin{bmatrix} \mathbf{K}_{ss}^{\Omega} & 0 & \mathbf{K}_{sb_1}^{\Omega} & \cdots & \mathbf{K}_{sb_{Nb}}^{\Omega} \\ 0 & \mathbf{K}_{dd}^{\Omega} & 0 & \cdots & 0 \\ \left(\mathbf{K}_{sb_1}^{\Omega}\right)^{\mathrm{T}} & 0 & \mathbf{K}_{b_1b_1}^{\Omega} & \ddots & \vdots \\ \vdots & \vdots & \ddots & \ddots & 0 \\ \left(\mathbf{K}_{sb_{Nb}}^{\Omega}\right)^{\mathrm{T}} & 0 & \cdots & 0 & \mathbf{K}_{b_{Nb}b_{Nb}}^{\Omega} \end{bmatrix}. \tag{A.9}$$

The element matrix are given as

$$\mathbf{M}_{ss}=\int_0^{L_s} I_s\boldsymbol{\Phi}^{\mathrm{T}}\boldsymbol{\Phi}\,\mathrm{d}Z+I_d\left[\boldsymbol{\Phi}^{\mathrm{T}}\boldsymbol{\Phi}\right]_{Z=Z_d}+\rho_bA_b\sum_{k=1}^{N_b}\int_{r_d}^{r_b}x_k^2\left[\boldsymbol{\Phi}^{\mathrm{T}}\boldsymbol{\Phi}\right]_{Z=Z_d}\mathrm{d}x_k, \tag{A.10}$$

$$\mathbf{M}_{sb_k}=\rho_bA_b\int_{r_d}^{r_b}x_k\boldsymbol{\Phi}^{\mathrm{T}}\big|_{Z=Z_d}\mathbf{V}_k\cos\beta\,\mathrm{d}x_k, \tag{A.11}$$

$$\mathbf{M}_{dd} = \rho_d h_d \int_{r_s}^{r_d}\int_0^{2\pi} \mathbf{W}^{\mathrm{T}}\mathbf{W} r\,\mathrm{d}r\,\mathrm{d}\theta + \rho_b A_b \sum_{k=1}^{N_b}\int_{r_d}^{r_b}\left\{ \left[\mathbf{W}^{\mathrm{T}}\mathbf{W}\right]_{\substack{r=r_d\\ \theta=\theta_k}} + x_k\left[\mathbf{W}^{\mathrm{T}}\frac{\partial \mathbf{W}}{\partial r} + \left(\frac{\partial \mathbf{W}}{\partial r}\right)^{\mathrm{T}}\mathbf{W}\right]_{\substack{r=r_d\\ \theta=\theta_k}} + x_k^2\left[\left(\frac{\partial \mathbf{W}}{\partial r}\right)^{\mathrm{T}}\frac{\partial \mathbf{W}}{\partial r}\right]_{\substack{r=r_d\\ \theta=\theta_k}}\right\}\mathrm{d}x_k, \tag{A.12}$$

$$\mathbf{M}_{db_k} = -\rho_b A_b \int_{r_d}^{r_b}\left[\mathbf{W}^{\mathrm{T}} + x_k\left(\frac{\partial \mathbf{W}}{\partial r}\right)^{\mathrm{T}}\right]_{\substack{r=r_d\\ \theta=\theta_k}}\mathbf{V}_k \sin\beta\,\mathrm{d}x_k, \tag{A.13}$$

$$\mathbf{M}_{b_k b_k} = \rho_b A_b \int_{r_d}^{r_b}\mathbf{V}_k^{\mathrm{T}}\mathbf{V}_k\,\mathrm{d}x_k, \tag{A.14}$$

$$\mathbf{P}_{dd} = \rho_d h_d \int_{r_s}^{r_d}\int_0^{2\pi}\left[\mathbf{W}^{\mathrm{T}}\frac{\partial \mathbf{W}}{\partial \theta} + \left(\frac{\partial \mathbf{W}}{\partial \theta}\right)^{\mathrm{T}}\mathbf{W}\right] r\,\mathrm{d}r\,\mathrm{d}\theta, \tag{A.15}$$

$$\mathbf{K}_{ss}^{e} = \int_0^{L_s} G_s J_s \mathbf{\Phi}'^{\mathrm{T}}\mathbf{\Phi}'\,\mathrm{d}Z, \tag{A.16}$$

$$\begin{aligned}\mathbf{K}_{dd}^{e} = {} & D\int_{r_s}^{r_d}\int_0^{2\pi} r\left(\nabla^2\mathbf{W}\right)^{\mathrm{T}}\left(\nabla^2\mathbf{W}\right)\mathrm{d}r\,\mathrm{d}\theta - (1-v)D\int_{r_s}^{r_d}\int_0^{2\pi}\left[\left(\frac{\partial^2\mathbf{W}}{\partial r^2}\right)^{\mathrm{T}}\left(\frac{\partial \mathbf{W}}{\partial r} + \frac{1}{r}\frac{\partial^2\mathbf{W}}{\partial\theta^2}\right)\right.\\ & \left. + \left(\frac{\partial \mathbf{W}}{\partial r} + \frac{1}{r}\frac{\partial^2\mathbf{W}}{\partial\theta^2}\right)^{\mathrm{T}}\frac{\partial^2\mathbf{W}}{\partial r^2}\right]\mathrm{d}r\,\mathrm{d}\theta\\ & + 2(1-v)D\int_{r_s}^{r_d}\int_0^{2\pi}\frac{1}{r}\left(\frac{\partial^2\mathbf{W}}{\partial r\partial\theta} - \frac{1}{r}\frac{\partial \mathbf{W}}{\partial\theta}\right)^{\mathrm{T}}\left(\frac{\partial^2\mathbf{W}}{\partial r\partial\theta} - \frac{1}{r}\frac{\partial \mathbf{W}}{\partial\theta}\right)\mathrm{d}r\,\mathrm{d}\theta,\end{aligned} \tag{A.17}$$

$$\mathbf{K}_{b_k b_k}^{e} = E_b I_{bA}\int_{r_d}^{r_b}\mathbf{V}''^{\mathrm{T}}_k\mathbf{V}''_k\,\mathrm{d}x_k, \tag{A.18}$$

$$\mathbf{K}_{dd}^{i} = h_d\int_{r_s}^{r_d}\int_0^{2\pi}\left[\sigma_r\left(\frac{\partial \mathbf{W}}{\partial r}\right)^{\mathrm{T}}\frac{\partial \mathbf{W}}{\partial r} + \frac{\sigma_\theta}{r^2}\left(\frac{\partial \mathbf{W}}{\partial\theta}\right)^{\mathrm{T}}\frac{\partial \mathbf{W}}{\partial\theta}\right]\mathrm{d}r\,\mathrm{d}\theta, \tag{A.19}$$

$$\mathbf{K}_{ss}^{\Omega} = \frac{1}{2}\rho_b A_b\sum_{k=1}^{N_b}\int_{r_d}^{r_b}\left(r_b^2 - 3x_k^2\right)\left[\mathbf{\Phi}^{\mathrm{T}}\mathbf{\Phi}\right]_{Z=Z_d}\mathrm{d}x_k, \tag{A.20}$$

$$\mathbf{K}_{sb_k}^{\Omega} = \rho_b A_b\left[\int_{r_d}^{r_b} x_k\mathbf{\Phi}^{\mathrm{T}}\big|_{Z=Z_d}\mathbf{V}_k\cos\beta\,\mathrm{d}x_k - \frac{1}{2}\int_{r_d}^{r_b}\left(r_b^2 - x_k^2\right)\mathbf{\Phi}^{\mathrm{T}}\big|_{Z=Z_d}\mathbf{V}'_k\cos\beta\,\mathrm{d}x_k\right], \tag{A.21}$$

$$\mathbf{K}_{dd}^{\Omega} = \rho_d h_d\int_{r_s}^{r_d}\int_0^{2\pi}\left(\frac{\partial \mathbf{W}}{\partial\theta}\right)^{\mathrm{T}}\frac{\partial \mathbf{W}}{\partial\theta} r\,\mathrm{d}r\,\mathrm{d}\theta, \tag{A.22}$$

$$\mathbf{K}_{b_k b_k}^{\Omega} = \rho_b A_b\int_{r_d}^{r_b}\mathbf{V}_k^{\mathrm{T}}\mathbf{V}_k\cos^2\beta\,\mathrm{d}x_k - \frac{1}{2}\rho_b A_b\int_{r_d}^{r_b}\left(r_b^2 - x_k^2\right)\mathbf{V}'^{\mathrm{T}}_k\mathbf{V}'_k\,\mathrm{d}x_k, \tag{A.23}$$

$$R_c = \frac{E_b I_A}{D(r_b - r_d)}. \tag{A.24}$$

References

[1] H. Lamband, R.V. Southwell, The vibrations of a spinning disk, *Proceedings of the Royal Society, London* 99 (1921) 272–280.
[2] R.V. Southwell, On the free transverse vibrations of a uniform circular disk clamped at its center; and on the effects of rotation, *Proceedings of the Royal Society, London* 101 (1921) 133–153.
[3] J.A. Dopkin, T.E. Shoup, Rotor resonant speed reduction caused by flexibility of disks, *ASME Journal of Engineering for Industry* 96 (1974) 1328–1333.
[4] I.Y. Shen, C.-P.R. Ku, A nonclassical vibration analysis of a multiple rotating disk and spindle assembly, *ASME Journal of Applied Mechanics* 64 (1997) 165–174.
[5] S.M. Vogel, D.W. Skinner, Natural frequencies of transversely vibration uniform annular plates, *ASME Journal of Applied Mechanics* 32 (1965) 926–931.
[6] R.L. Eshleman, R.A. Eubanks, On the critical speeds of a continuous shaft–disk system, *ASME Journal of Engineering for Industry* 89 (1967) 645–652.
[7] R.M. Laurenson, Modal analysis of rotating flexible structure, *AIAA Journal* 14 (10) (1976) 1444–1450.
[8] H.N. Ozguven, On the critical speed of continuous shaft-disk systems, *ASME Journal of Vibration and Acoustics* 106 (1984) 59–61.
[9] F. Sisto, A. Chang, M. Sutcu, The influence of coriolis forces on gyroscopic motion of spinning blades, *ASME Journal of Engineering for Power* 105 (1983) 342–347.
[10] K.B. Subrahmanyam, K.R.V. Kaza, Vibration and buckling of rotating pretwisted, preconed beams including coriolis effects, *ASME Journal of Vibration, Acoustics, Stress, and Reliability in Design* 108 (1986) 140–149.
[11] D.J. Ewins, Vibration characteristics of bladed disc assemblies, *Journal of Mechanical Engineer Science* 15 (3) (1973) 165–185.
[12] F. Kushner, Disc vibration-rotating blade and stationary vane interaction, *Journal of Mechanical Design* 102 (1980) 579–584.
[13] D.R. Chivens, H.D. Nelson, The natural frequencies and critical speeds of a rotating, flexible shaft–disk system, *ASME Journal of Engineering for Industry* 97 (1975) 881–886.
[14] A.A.S. Shahab, J. Thomas, Coupling effects of disc flexibility on the dynamic behaviour of multi disc–shaft systems, *Journal of Sound and Vibration* 114 (1987) 435–452.
[15] I.Y. Shen, Closed-form forced response of a damped, rotating multiple disk/spindle system, *ASME Journal of Applied Mechanics* 64 (1997) 343–352.
[16] F. Wu, G.T. Flowers, A transfer matrix technique for evaluating the natural frequencies and critical speeds of a rotor with multiple flexible disks, *ASME Journal of Vibration and Acoustics* 114 (1992) 242–248.
[17] H.S. Jia, S.B. Chun, C.W. Lee, Evaluation of the longitudinal coupled vibrations in rotating, flexible disks/spindle systems, *Journal of Sound and Vibration* 208 (1997) 175–187.
[18] C.W. Lee, S.B. Chun, Vibration analysis of a rotor with multiple flexible disks using assumed modes method, *ASME Journal of Vibration and Acoustics* 120 (1998) 87–94.
[19] V. Omprakash, V. Ramamurti, Natural frequencies of bladed disks by a combined cyclic symmetry and rayleigh–ritz method, *Journal of Sound and Vibration* 125 (2) (1988) 357–366.
[20] V. Omprakash, V. Ramamurti, Coupled free vibration characteristics of rotating tuned bladed disk systems, *Journal of Sound and Vibration* 140 (3) (1990) 413–435.
[21] N. Khader, R.G. Loewy, Shaft flexibility effects on the forced response of a blade-disk assembly, *Journal of Sound and Vibration* 139 (1990) 469–485.
[22] M. Sakata, K. Kimura, S.K. Park, Vibration of bladed flexible rotor due to gyroscopic moment, *Journal of Sound and Vibration* 131 (1989) 417–430.
[23] S.B. Chun, C.W. Lee, Vibration of shaft–bladed disk system by using substructure synthesis and assumed modes method, *Journal of Sound and Vibration* 189 (1996) 587–608.
[24] S.C. Huang, K.B. Ho, Coupled shaft–torsion and blade–bending vibrations of a rotating shaft–disk–blade unit, *ASME Journal of Engineering for Gas Turbines and Power* 118 (1996) 100–106.
[25] C. H. Yang, S. C. Huang, Coupling vibrations in rotating shaft–disk–blades system, *ASME Journal of Vibration and Acoustics* 2004, revised.
[26] S.C. Huang, W. Soedel, Effects of coriolis acceleration on the free and forced in-plane vibrations of rotating rings on elastic foundation, *Journal of Sound and Vibration* 115 (1987) 253–274.